Reaction $^{27}Al + \alpha$ at $E_\alpha = 140$ MeV: I

M. D. Glascock,* W. F. Hornyak, C. C. Chang, and R. J. Quickle†
University of Maryland Cyclotron Laboratory, College Park, Maryland 20742
(Received 30 August 1978)

Detailed results of the investigation of the in-beam γ rays from 140 MeV α particles incident on the deformed nucleus ^{27}Al are presented. They are supplemented by experimental evidence obtained from the observed differential cross section measurements for p, d, t, h, and α particles in the discrete portion of the energy spectra. Striking spectroscopic similarities are observed for the strongly excited states in residual nuclei both near and considerably removed in N and Z from the target nucleus. Some of these involve related collective states exhibiting strong quadrupole excitations.

NUCLEAR REACTIONS ^{27}Al(α, p), (α, d), (α, t), (α, h), (α, α'), (α, x-γ), E_α = 140 MeV; measured E_γ, σ_γ, cross sections for producing specific levels in residual nuclei, Doppler broadening, $\sigma(\theta, E)$ for discrete energy groups p, d, t, h, α; deduce reaction channel characteristics. Ge(Li) detector.

I. INTRODUCTION

A comprehensive set of experiments[1,2] was undertaken to investigate the reaction mechanism characteristics operating when energetic α particles are incident on a deformed nucleus. Another motivation was the desire to bridge the gap between the extensive studies that exist for protons and heavy ions used as projectiles. The limited fragmentation possibilities of the α particle compared to heavier ions also allows for an easier interpretation of the complex residual nucleus spectrum produced. The deformed target nucleus ^{27}Al was selected primarily because of the substantial amount of known information concerning possible levels in expected residual nuclei.

Statistical model calculations have attempted to account for the major features of reactions such as the one studied here in terms of a combination of pre-equilibrium and evaporation processes.[3-6] It was also felt desirable to establish the limits of validity of such models for the present case.

Experiments involving the detection of *in-situ* γ rays, charged-light particles with $A \leq 4$, and heavier ions with $A > 4$ were undertaken in this laboratory. The results for p, d, t, h, and α particles in the continuum region are reported elsewhere.[7] Experimental results for these particles in the discrete region of the energy spectrum and the experimental γ-ray results bearing on specific nuclear states are reported in this paper. Results obtained from the detection of ions with $A > 4$ without regard for individual level information, various theoretical calculations, and general conclusions are reported in Ref. 8. It is found that the combination of such data permits a satisfactory determination of the main features of the various reaction processes. A more detailed explanation of these results is described in Refs. 1 and 2.

II. EXPERIMENTAL METHOD

The experiment was conducted at the University of Maryland cyclotron facility on a low background station especially designed for γ-ray measurements. Most of the γ-ray data were acquired using an aluminum foil target with a thickness of 14.2 mg/cm^2, mounted in a hydrocarbon plastic frame. The beam spot on the target was generally of order 2×2 mm. A total charge of 28 μC was accumulated during the main experimental run. To further eliminate possible extraneous background, this run was taken in part with a thick lead collimator and shield and in part without any collimation. With the collimator and shield in place, only the plastic target box windows and target frame could be seen by the γ-ray detector.

A software computer program[9] was developed that permits timing information to be obtained using the cyclotron beam fine structure as a time reference for the observed γ-ray events. Fast timing measurements indicate a cyclotron fine structure beam burst width (for the generally obtainable single turn extraction) of less than 1.2 ns repeated in the case of 140-MeV α particles every 90 ns. Twelve contiguous analyzers with adjustable time widths may be set as desired with reference to the RF stop signal generating the time-to-amplitude converter (TAC) output.

Figure 1 shows the TAC output spectrum obtained during an *in-situ*, γ-ray run. The prompt

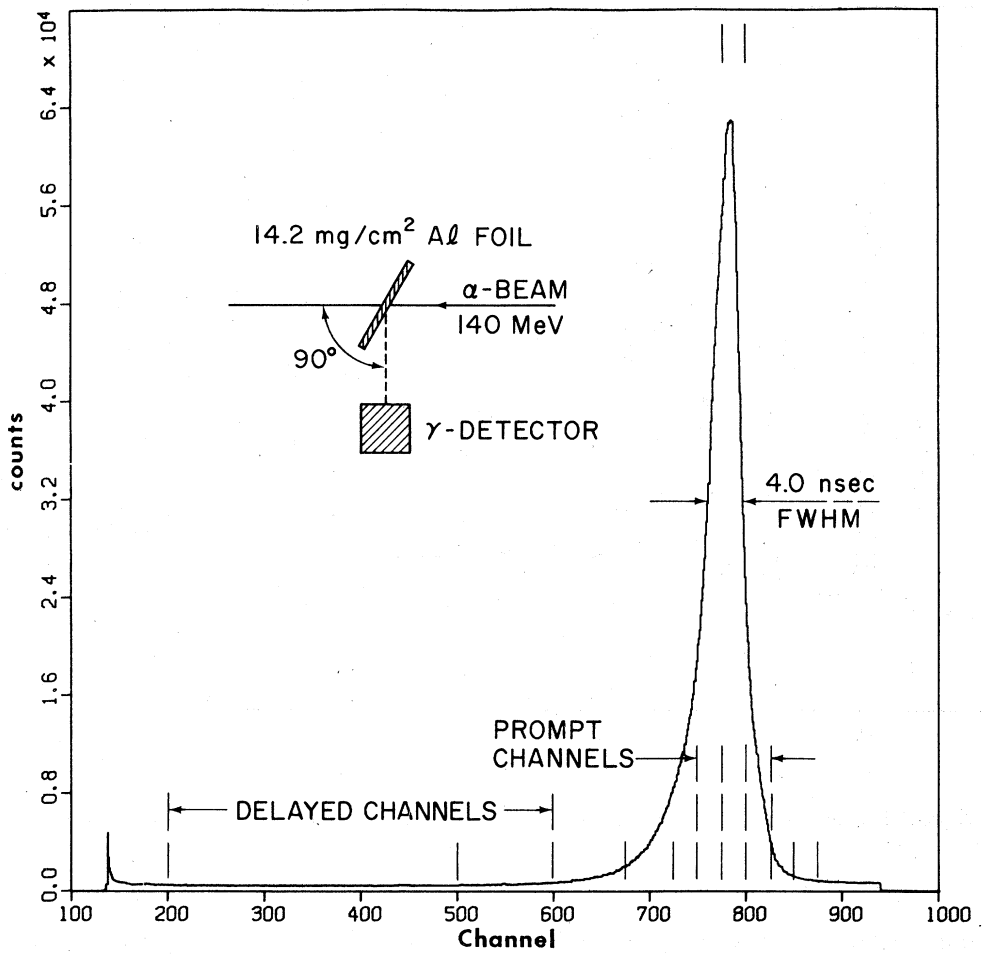

FIG. 1. The time-to-amplitude (TAC) spectrum with *in-situ* γ rays providing start events and the cyclotron rf providing the stop events. The twelve derived time windows are indicated, three narrow windows (7.5 ns) for determining the so-called prompt events and the wide window (40 ns) for the so-called delayed events.

γ-ray events occur within a peak having a time width equal to 4.0 ns (FWHM). Several 2.5 ns wide channels were set covering this peak and a few other wider channels were set to its delayed time side, allowing the observation of γ-ray spectra originating within a number of short time intervals after the beam strikes the target.

Throughout, we refer to spectral lines associated with the three channels totalling 7.5 ns in width and centered on the TAC peak as the *prompt* spectrum. A very broad 40-ns-wide window is set to give the major information on the time *delayed* spectrum. This delayed window includes radioactive events, long-lived meta-stable decays, and the neutron-induced secondary reactions within the γ-ray detector itself. A slow-rise-time (SRT)-reject circuit was used to eliminate γ-ray pulses giving artificially delayed time signatures due to the long collection time for charge carriers in the detector. This is particularly severe for low energy events.

A coaxial Ge(Li) detector, with 10% efficiency relative to a 7.6×7.6 cm NaI detector at 25 cm, was used to detect γ rays up to 10 MeV in energy. A planar intrinsic Ge detector (2.5 cm D ×1.0 cm$H$) was used for detecting the lowest-energy γ rays. With the SRT-reject circuit, useful timing information was available down to ≈30 keV with this detector. Figure 2 shows a portion of the prompt spectrum obtained with the Ge(Li) coaxial detector.

Absolute efficiencies for the detectors were determined up to an energy of 2615 keV using numerous radioactive sources placed in the target position. The efficiencies were extended up to 10 MeV for the Ge(Li) coaxial detector from calculations based on results reported in the literature for comparable detectors.[10-12] Figure 3 shows a portion of the high-energy spectrum obtained for

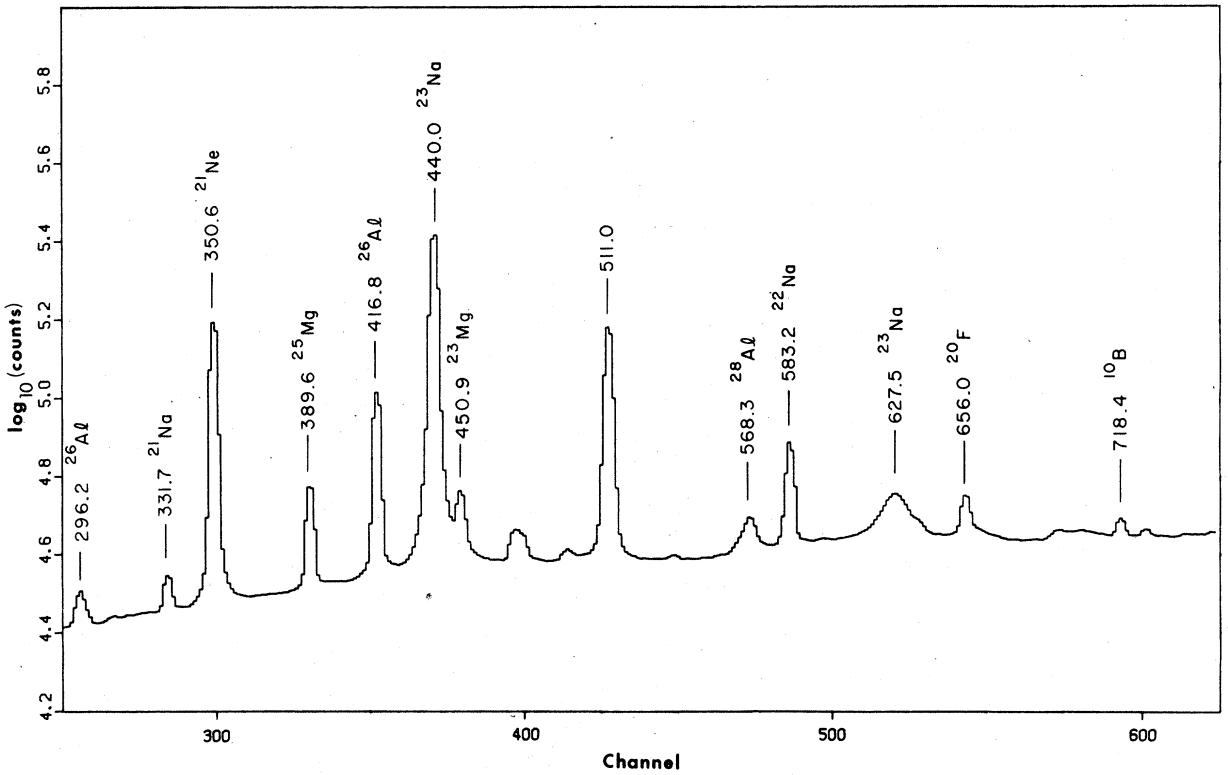

FIG. 2. A portion of the low-energy, prompt, *in-situ*, γ-ray spectrum with prominent lines identified. Energies are indicated in keV.

this detector. Relatively weak lines not too severely Doppler broadened, such as the 6.246-MeV line in ^{24}Mg (width, FWHM ≈7 keV) with a cross section $\sigma_\gamma = 0.35$ mb, may be readily observed. The absolute efficiency of this detector varied from 5×10^{-4} at 500 keV to 5×10^{-5} at 8 MeV. The coaxial detector resolution of 2.0 keV at 1 MeV and the overall stability of the electronics permitted γ-ray energies to be determined to better than ±0.2 keV in the delayed spectra where there is little Doppler broadening. The planar detector had less than 1 keV resolution throughout the range below 500 keV.

A comparison of the two collimator arrangements is shown in Fig. 4. The upper curve is for a run with the lead collimator and shield, while the lower one is for a run without collimation. The comparison is necessary, primarily to establish the fact that no significant contribution to the prompt spectrum arises from any stray or scattered beam striking the beam transport system during the *in-situ* runs. In addition, careful stripping of the important 3004-keV line in ^{27}Al from the spectrum in all time slices and with both collimator geometries showed that within the ability to define the background, the events allocated to the prompt time window was the same for both geometries. However, for the uncollimated geometry, there were some 3–5 % additional events in the time window 5 ns later than the TAC peak (and outside the selected prompt window) which were also low-energy skewed. Except for the above effects, the similarity of the two curves in Fig. 4 demonstrates the essentially pure, target-related nature of the detected γ-ray events.

The data were accumulated and stored on tape, with the IBM 360/44 on-line computed facility at the University of Maryland cyclotron, utilizing a software program developed at this laboratory.[9] Data striping for peak locations, widths, areas, and their errors were found, using a light-pen interactive program PEAK2[13] based on the analysis of Mariscotti.[14]

The extensive data collected by the group of Ref. 7 also included information on protons, deuterons, tritons, ^{3}He, and α particles with discrete energies indicating two-body processes with excitation energies up to 15 MeV in the residual nuclei. The relevant data tapes were made available for de-

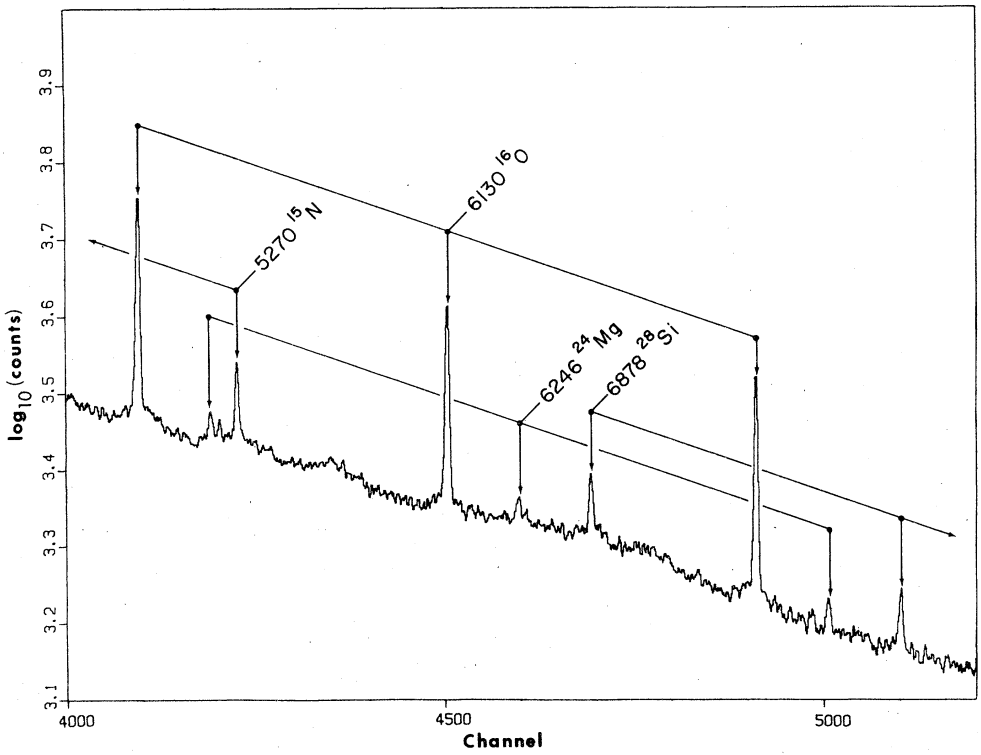

FIG. 3. A portion of the high-energy, prompt, *in-situ*, γ-ray spectrum with prominent lines identified. The energies are indicated in keV. The weakest γ ray indicated is determined to have a cross section of $\sigma_\gamma = 350$ mb.

tailed analysis for present purposes.

These light particles were observed in a 1.5-m scattering chamber, employing two separate externally rotatable detector arms. One arm carried a particle telescope with a 500 μm thick Si ΔE-detector and a 4-mm thick Si(Li) E detector (set at a 60° angle) for charge-two particles, while the other arm held a telescope consisting of two Si ΔE-detectors, one 100 μm thick and the other 1 mm thick, followed by a 7.6 cm NaI crystal E detector for detecting singly charged particles. The energy calibration of these telescope elements permitted a computer software program to give unique particle-type identification.

A thin ^{27}Al target of 1.72 mg/cm^2 was used in the main experimental runs with charge accumulation in the range 30–40 μC. The two telescopes subtended similar solid angles of order 2.5×10^{-4} sr. At small angles the angular distribution was taken at 5° intervals with larger steps beyond a laboratory angle of 45°.

III. EXPERIMENTAL RESULTS

Over 170 prompt γ-ray lines attributable to the primary target reaction were observed, and all identified. In addition, over 40 delayed lines were also identified. Prompt γ-ray production cross sections were observed to range from a high of 78 mb to an average lowest detectable value of a few hundred microbarns. An additional possible 50 γ-ray lines were assigned upper limits for their production cross sections.

Table I presents the resultant cross sections for the production of particular excited states in each residual nucleus by direct excitation and/or by γ feeding from unidentified higher lying states. γ feeding by transitions from identified states has been subtracted. The observed linewidths (FWHM) are also in kilovolts; when no significant Doppler broadening is evident, the linewidth is referred to as standard (STD). The γ-ray cross sections are computed on the assumption of isotropic angular distributions. Table II presents the resultant cross sections for ground-state β decays deduced from the delayed spectra. Production cross section for a particular residual nucleus based solely on the observed γ-ray intensities will be referred to as gamma-ray-based (GRB) cross section. These of course fail to include any direct ground state population and may miss weak transitions, particularly for Doppler-broadened, high-energy

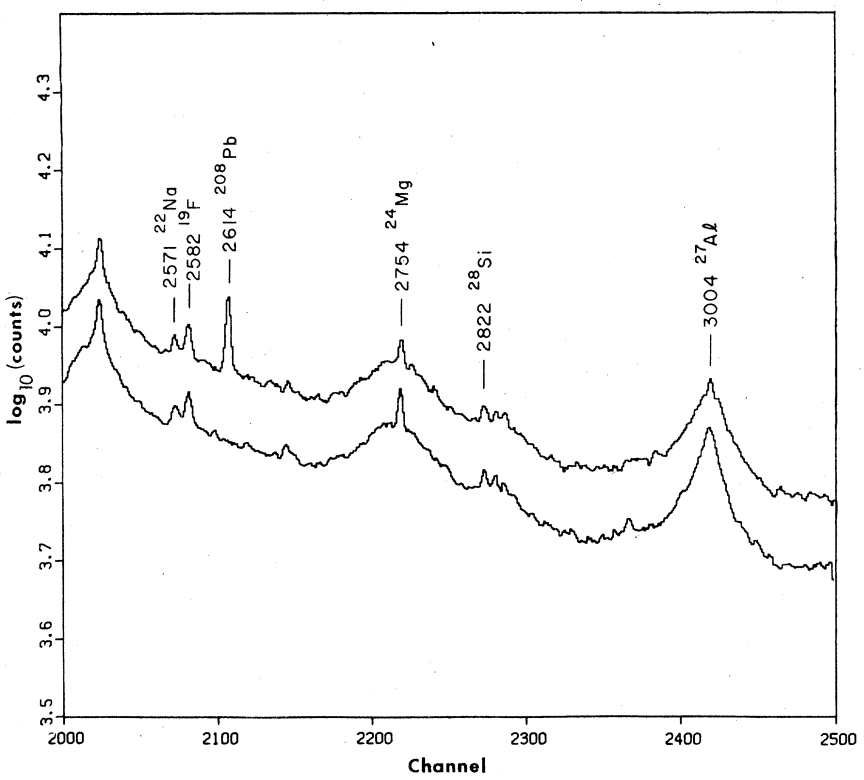

FIG. 4. Corresponding portions of the midenergy, prompt, *in-situ*, γ-ray spectra with prominent lines identified. The energies are indicated in keV. The upper spectrum was obtained with a thick lead collimator and shield, the lower spectrum without collimation. The upper curve has been shifted upwards by 0.10 $\log_{10}$ units in order to separate the two curves which were taken for the same integrated beam charge.

γ rays. In the case of β-decay-produced γ rays all cascading and direct ground state population are of course included. γ rays were identified with the decay of particular residual nucleus levels by using the excitation energy, lifetime, and branching ratio compilations.[15-17]

Most of the lines in the prompt spectrum showed Doppler broadening, particularly if the relevant lifetime was under a picosecond. All of the data were taken at 90° to the beam direction, thus producing only symmetrically broadened lines. The extreme difficulty of reliably fitting the shifted and distorted Doppler shapes for angles other than 90° would prevent detection of anisotropies as large as 25%. The Ge(Li) detector at 90° subtended a cone with a half angle of 13° which corresponds to an effective solid angle of 23% of a sphere due to the presence of axial symmetry. The quoted γ-ray yields based on assumed isotropy might have an estimated uncertainty of the order of 20%. For example, the production yields for ^{28}Al and ^{24}Na as deduced from prompt γ-ray yields agree rather well with the β-decay yields (provided a small allowance is made for unobservable direct ground state production).

The discrete line spectra for high-energy α's, ^{3}He, tritons, and deuterons from the corresponding (α,α'), (α,h), (α,t), and (α,d) reactions are presented in Figs. 5, 6, 7, and 8, respectively. The excitation energies and corresponding angle-integrated cross sections are given.

Finally, the results for the total production cross section of residual nuclei in the inclusive reactions ^{27}Al(α,x) at E_α = 140 MeV are given in Fig. 9. These values are based only on γ-ray evidence for lines actually observed as detailed above. No estimates based on upper limits for masked lines are included. The quoted results do not include nuclear events directly feeding the ground states or unobserved transitions to the ground state from weakly excited levels, particularly those involving high-energy γ rays that might be considerably Doppler broadened. The exception is for β-decaying nuclei for which the delayed γ rays in the daughter have been observed. These values have an asterisk label in Fig. 9.

TABLE I. Cross sections from prompt spectra for 140-MeV α particles interacting with ^{27}Al.

Residual nucleus	E_{ex} (MeV)	J^{π}	Final level	Linewidth (keV)	σ_{γ} [a] (mb)	σ_{x} [b] (mb)
^{7}Li	0.478(I)	$\frac{1}{2}^-$	0		c	≤2
^{7}Be	0.429(I)	$\frac{1}{2}^-$	0		c	≤2
^{8}Li	0.981(I)	1^+	0		d	≤2
^{10}B	0.718(I)	1^+	0	STD	1.2	1.2
^{11}B	2.124(I)	$\frac{1}{2}^-$	0		c	≤0.5
^{12}B	0.953(I)	2^+	0		c	≤0.4
^{12}C	4.439(I)	2^+	0	100	2	2
^{13}C	3.853(I)	$\frac{5}{2}^+$	0	STD	0.7	1.1
^{14}C	6.728(I)	3^-	0	STD	0.07	0.07
^{14}N	2.311(I)	0^+	0	6	0.7	0.7
	5.106(II)	2^-	0	7	1	0.5
	5.832(III)	3^-	0, II	10, STD	0.1, 0.5	0.6
^{15}N	5.269(I)	$\frac{5}{2}^+$	0	5.8	1.1	1.1
	5.299(II)	$\frac{1}{2}^+$	0		c	≤0.3
^{15}O	5.183(I)	$\frac{1}{2}^+$	0	STD	≤0.2	≈0.0
	5.239(II)	$\frac{5}{2}^+$	I	STD	0.2	0.2
^{16}O	6.129(I)	3^-	0	7.5	4.0	4.0
	6.917(II)	2^+	0		c	≤1
	7.117(III)	1^-	0		c	≤1
	8.870(IV)	2^-	I, III	all STD	d, 0.7	≤5
^{17}N	1.370(I)	$\frac{5}{2}^-$	0		c	≤2
^{17}O	0.871(I)	$\frac{1}{2}^+$	0	STD	2.0	2.0
	3.060(II)	$\frac{1}{2}^-$	I		c	≤2
	3.850(III)	$\frac{5}{2}^-$	0		c	≤1
^{17}F	0.496(I)	$\frac{1}{2}^+$	0	STD	0.2	0.2
^{18}O	1.982(I)	2^+	0	STD	2.5	2.5
^{18}F	0.937(I)	3^+	0	STD	2.7	2.2
	1.042(II)	0^+	0	5	0.5	≤0.1
	1.081(III)	0^-	0	STD	0.4	≤0.1
	1.122(IV)	5^+	0		d	≤0.2
	1.701(V)	1^+	0, II	4.6, STD	0.3, 0.6	0.9
	2.101(VI)	2^-	0, I	5, 3.2	0.5, 0.5	1.5
	2.524(VII)	2^+	0		c	≤1
	3.060(VIII)	2^+	II		c	≤0.5
^{18}Ne	1.887(I)	2^+	0		c	≤0.4
^{19}F	0.110(I)	$\frac{1}{2}^-$	0	STD	8.0	4.9
	0.197(II)	$\frac{5}{2}^+$	0	STD	32	30
	1.346(III)	$\frac{5}{2}^-$	I	STD	3.1	3.1
	1.459(IV)	$\frac{3}{2}^-$	I		d	≤3

TABLE I. *(Continued)*.

Residual nucleus	E_{ex} (MeV)	J^π	Final level	Linewidth (keV)	σ_γ [a] (mb)	σ_x [b] (mb)
	1.554(V)	$\frac{3}{2}^+$	I		d	≤10
	2.780(VI)	$\frac{9}{2}^+$	II	5.5	1.3	0.2
	3.907(VII)	$\frac{3}{2}^{(+)}$	0		c	≤5
	4.648(VIII)	$\frac{13}{2}^+$	VI	5.9	1.1	1.1
^{19}Ne	0.238(I)	$\frac{5}{2}^+$	0	STD	0.5	0.5
	0.275(II)	$\frac{1}{2}^-$	0	STD	1.4	1.4
^{20}F	0.656(I)	3^+	0	STD	2.8	0.8
	0.823(II)	$(2^+, 4^+)$	0, I	all STD	0.9, 2	2.9
^{20}Ne	1.634(I)	2^+	0	7	13.3	11.8
	4.967(II)	2^-	I	4.0	1.5	1.5
^{21}F	0.280(I)	$\frac{1}{2}^+$	0		c	≤0.1
^{21}Ne	0.351(I)	$\frac{5}{2}^+$	0	STD	35	≤3
	1.746(II)	$\frac{7}{2}^+$	I	45	25	11
	2.789(III)	$\frac{1}{2}^-$	I	STD	0.5	0.6
	2.796(IV)	$\frac{1}{2}^+$	0		c	≤1
	2.866(V)	$\frac{9}{2}^+$	I, II	30, 35	8, 15	23
	3.662(VI)	$\frac{3}{2}^-$	I		c	≤0.5
	3.734(VII)	$\frac{5}{2}^+$	I		c	≤1
	3.883(VIII)	$\frac{5}{2}$	I		c	≤1
	4.432(IX)	$\frac{11}{2}^+$	V		c	≤2
	5.525(X)	$\frac{9}{2}^+$	II		c	≤1
^{21}Na	0.332(I)	$\frac{5}{2}^+$	0	STD	1.7	1.7
^{22}Ne	1.275(I)	2^+	0	STD	15.8	8.1
	3.357(II)	4^+	I	28	5.4	5.4
	4.457(III)	2^+	I	15	0.6	0.1
	5.144(IV)	2^-	I, III	all STD	0.3, 0.5	0.8
	5.335(V)	$(1, 2)^+$	I	4	0.3	0.7
	5.360(VI)	2^+	I	13	1.1	1.1
	5.523(VII)	4^+	I		c	≤0.5
	5.641(VIII)	3^+	I		c	≤0.6
	5.914(IX)	2^+	I		c	≤0.3
	6.305(X)	6^+	II		d	≤1
	7.537(XI)	$(4, 5)^+$	VIII		c	≤0.6
	11.010(XII)	(6, 8)	X	15	0.5	0.5
^{22}Na	0.583(I)	1^+	0	STD	15	≤1
	0.657(II)	0^+	I	STD	1.4	0.5
	0.891(III)	4^+	0	STD	5.7	5.5
	1.528(IV)	5^+	0, III	all STD	4.2, 0.3	4.4
	1.937(V)	1^+	II		c	≤1
	1.952(VI)	2^+	I	52	15	14

TABLE I. *(Continued)*.

Residual nucleus	E_{ex} (MeV)	J^{π}	Final level	Linewidth (keV)	σ_{γ} [a] (mb)	σ_{x} [b] (mb)
	1.983(VII)	3^+	I	STD	16	1.6
	2.212(VIII)	1^-	II	STD	0.9	0.5
	2.572(IX)	2^-	0	STD	0.7	0.9
	2.969(X)	3^+	VI		d	≤2
	3.060(XI)	2^+	VI		d	≤2
	3.521(XII)	3^-	VI, VIII	3, 4	0.9, 0.4	1.7
	3.708(XIII)	6^+	IV		c	≤0.4
	3.945(XIV)	1^+	I		c	≤0.3
^{22}Mg	1.247(I)	2^+	0		c	≤0.2
^{23}Na	0.440(I)	$\frac{5}{2}^+$	0	STD	62.3	6
	2.076(II)	$\frac{7}{2}^+$	I	30	38	26.2
	2.391(III)	$\frac{1}{2}^+$	0		c	≤1.5
	2.640(IV)	$\frac{1}{2}^-$	0		c	≤0.2
	2.704(V)	$\frac{9}{2}^+$	I, II	40, 13	18, 9.9	21.3
	2.982(VI)	$\frac{3}{2}^+$	0		c	≤0.6
	3.678(VII)	$\frac{3}{2}^-$	I		c	≤0.8
	3.848(VIII)	$\frac{5}{2}^-$	II		c	≤2.5
	3.915(IX)	$\frac{5}{2}^+$	0	120	9.0	11
	5.536(X)	$(\frac{7}{2}, \frac{9}{2}, \frac{11}{2})^+$	II, V	20, 50	≈1, 6.6	8.0
	6.236(XI)	$(\frac{9}{2}, \frac{13}{2})$	V		c	≤2
^{23}Mg	0.451(I)	$\frac{5}{2}^+$	0	STD	2	1.7
	3.795(II)	$\frac{3}{2}^-$	0	6	0.3	0.3
^{24}Na	0.473(I)	1^+	0	STD	13.5	8.1
	0.563(II)	2^+	I	STD	4.5	2.7
	1.341(III)	$2^{(+)}$	II	10	1	1
	1.345(IV)	$3^{(+)}$	0, II	3, 3.6	0.4, 0.5	1
	1.347(V)	1^+	I	STD	0.9	0.9
	1.512(VI)	$(3^+), 5^+$	0		c	≤0.5
	1.846(VII)	2^+	IV		c	≤1
	3.217(VIII)	$(2, 4)^+$	IV	5.9	1.1	1.1
	3.657(IX)	2^+	II	13	0.3	0.5
^{24}Mg	1.369(I)	2^+	0	15	78	50
	4.123(II)	4^+	I	69	28.0	28
	4.238(III)	2^+	0		c	≤1.5
	5.236(IV)	3^+	I		c	≤1.5
	6.010(V)	4^+	I		c	≤0.3
	6.431(VI)	0^+	I		c	≤0.7
	7.348(VII)	2^+	0		c	≤2
	7.553(VIII)	1^-	0		c	≤1.5
	7.616(IX)	3^-	0, I	7, 7	0.2, 0.4	0.6

TABLE I. *(Continued)*.

Residual nucleus	E_{ex} (MeV)	J^π	Final level	Linewidth (keV)	σ_γ [a] (mb)	σ_x [b] (mb)
	8.120(X)	(6^+)	II		d	≤3
	9.299(XI)	$(4)^-$	II		c	≤0.2
^{25}Na	0.089(I)	$(\frac{3}{2},\frac{5}{2})^+$	0		c	≤0.3
^{25}Mg	0.585(I)	$\frac{1}{2}^+$	0	STD	12.0	4.6
	0.975(II)	$\frac{3}{2}^+$	0, I	STD	6.0, 5.7	8.5
	1.612(III)	$\frac{7}{2}^+$	0	20	14	11.5
	1.965(IV)	$\frac{5}{2}^+$	0, I, II	4.0, 4.0, STD	0.8, 1.7, 0.6	2.8
	2.564(V)	$\frac{1}{2}^+$	I		c	≤1
	2.734(VI)	$\frac{7}{2}^+$	II	17	2.6	3.1
	2.801(VII)	$\frac{3}{2}^+$	0		c	≤0.4
	3.405(VIII)	$\frac{9}{2}^+$	0, III	8, 3.5	0.5, 2.5	1.2
	3.414(IX)	$\frac{3}{2}^-$	I		c	≤0.5
	3.903(X)	$(\frac{3}{2}^+,\frac{5}{2}^+)$	I		c	≤0.2
	3.966(XI)	$\frac{7}{2}^-$	0		c	≤0.6
	4.055(XII)	$\frac{9}{2}^+$	0		c	≤0.2
	5.245(XIII)	$(\frac{7}{2}^+)\frac{11}{2}^+$	0		c	≤0.6
	5.455(XIV)	$\frac{9}{2},\frac{13}{2}$	VIII	STD	1.8	2.0
^{25}Al	0.451(I)	$\frac{1}{2}^+$	0	STD	4	1.2
	0.945(II)	$\frac{3}{2}^+$	0, I	all STD	0.6, 0.6	≈0
	1.613(III)	$(\frac{7}{2})^+$	0	20	10	7
	1.790(IV)	$\frac{5}{2}^+$	0, II	20, 5.0	2.0, 2	6.6
	2.485(V)	$\frac{1}{2}^+$	I		c	≤0.1
	2.673(VI)	$\frac{3}{2}^+$	IV		c	≤0.4
	2.721(VII)	$\frac{7}{2}$	I		c	≤0.4
	3.424(VIII)	$(\frac{9}{2})^+$	0, III	–, 20	0.5, 3	3.5
	4.025(IX)	$(\frac{5}{2}^+,\frac{9}{2}^+)$	0		c	≤0.3
^{26}Mg	1.809(I)	2^+	0	13.5	60.4	34.2
	2.938(II)	2^+	0, I	27, 14	1.9, 16.6	14
	3.588(III)	0^+	I	STD	5.7	5.7
	3.941(IV)	3^+	I, II	8, 5	1.8, 3	5
	4.320(V)	4^+	I	5	2.1	2.1
	4.332(VI)	$(2)^+$	I		d	≤4
	4.350(VII)	3^+	I		c	≤1.5
	4.835(VIII)	2^+	II	17	1.6	1.9
	4.901(IX)	4^+	I		c	≤0.3
	4.972(X)	0^+	II		c	≤0.1
^{26}Al	0.228(I)	0^+	e			
	0.417(II)	3^+	0	STD	14.7	8.3
	1.058(III)	1^+	I	13.8	13.2	7.4
	1.759(IV)	2^+	II	STD	1.9	2.0

TABLE I. *(Continued)*.

Residual nucleus	E_{ex} (MeV)	J^{π}	Final level	Linewidth (keV)	σ_{γ} [a] (mb)	σ_{x} [b] (mb)
	1.850(V)	1^+	I		d	≤2
	2.0687(VI)	4^+	II	STD	0.7	1
	2.0695(VII)	2^+	II, III	10, 4.5	2, 4.7	≤0.1
	2.072(VIII)	1^+	I	6	1	1
	2.365(IX)	3^+	II, III, VII	all STD	0.5, 0.4, 2.0	3.5
	2.545(X)	3^+	VII	STD	1.6	2.6
	2.661(XI)	$(2, 3)^+$	II	5	0.5	0.8
	2.739(XII)	1^+	I	30	5.5	5.5
	2.913(XIII)	2^+	VII		c	≤1
	3.073(XIV)	$(2, 3)^+$	VII	6	2.4	2.8
	3.160(XV)	2^+	II		c	≤2
	3.403(XVI)	5^+	0		c	≤0.8
	3.508(XVII)	6^+	0		c	≤0.2
	3.596(XVIII)	$(2, 3)^+$	VII	22	4.9	6.1
	3.918(XIX)	$(5^+)7^+$	0		d	≤2
^{27}Mg	0.984(I)	$\frac{3}{2}^+$	0	STD	2.0	2.0
	1.698(II)	$\frac{5}{2}^+$	0	STD	1.4	1.4
^{27}Al	0.844(I)	$\frac{1}{2}^+$	0	STD	15.2	13.0
	1.015(II)	$\frac{3}{2}^+$	0, I	all STD	21.2, 0.6	18.3
	2.211(III)	$\frac{7}{2}^+$	0	39	33.4	25.2
	2.734(IV)	$\frac{5}{2}^+$	0, II	−, 21	d, 2.9	3.9
	2.981(V)	$\frac{3}{2}^+$	0		d	≤0.5
	3.004(VI)	$\frac{9}{2}^+$	0, III	51, 11	24.0, 2	21.3
	3.678(VII)	$\frac{1}{2}^+$	I, II	50, 8	1.2, 0.7	1.9
	3.956(VIII)	$(\frac{3}{2}, \frac{5}{2})^+$	0		c	≤0.8
	4.054(IX)	$(\frac{1}{2}, \frac{3}{2})^-$	I	40	1	1.2
	4.409(X)	$\frac{5}{2}^+$	0		c	≤0.3
	4.510(XI)	$\frac{11}{2}^+$	III, VI	9.8, 8	3, 2.7	5.2
	4.580(XII)	$\frac{7}{2}^+$	0	10	0.4	≤0.5
	4.812(XIII)	$\frac{5}{2}$	0		c	≤0.5
	5.432(XIV)	$\frac{9}{2}^+$	0, III	69, 30	2.1, 3	5
	5.500(XV)	$\frac{11}{2}^+$	VI		d	≤1
	6.464(XVI)	$\frac{7}{2}^-$	0		c	≤0.5
	6.512(XVII)	$\frac{11}{2}^+$	XI		c	1
	6.605(XVIII)	$\frac{1}{2}^+$	III		c	≤0.8
	6.651(XIX)	$\frac{5}{2}^-$	0		c	≤0.5
	7.399(XX)	$\frac{9}{2}$	XII		d	≤0.5
	7.443(XXI)	$(\frac{9}{2}, \frac{13}{2})^+$	VI, XV		c, c	≤4
^{27}Si	0.780(I)	$\frac{1}{2}^+$	0	4	0.5	0.5
	0.957(II)	$\frac{3}{2}^+$	0	4	1.4	1.4

TABLE I. *(Continued)*.

Residual nucleus	E_{ex} (MeV)	J^π	Final level	Linewidth (keV)	σ_γ [a] (mb)	σ_x [b] (mb)
^{28}Al	0.031(I)	2^+	0	STD	2.0	0.3
	0.972(II)	0^+	I	STD	0.4	0.4
	1.014(III)	3^+	I		c	≤0.2
	1.373(IV)	1^+	I		c	≤0.1
	1.620(V)	1^+	I	7	0.8	0.9
	1.623(VI)	$(2,3)^+$	0		d	≤3
	2.139(VII)	2^+	0, I		c, c	≤0.2
	2.202(VIII)	1^+	I	15	0.5	0.6
	2.272(IX)	4^+	0	40	13	11
	2.485(X)	2^+	V		c	≤0.2
	2.582(XI)	5^+	0, IX	6, 3	1.4, 0.2	1.5
	3.105(XII)	1^+	I		c	≤0.2
	3.465(XIII)	4^-	0	25	3.1	1.3
	4.033(XIV)	5^-	XI, XIII	−, 4	d, 1.8	3.5
	5.165(XV)	6^-	XIV		d	≤5
^{28}Si	1.779(I)	2^+	0	29	23.6	19
	4.618(II)	4^+	I	STD	0.3	≤0.1
	4.979(III)	0^+	I		d	≤2
	6.277(IV)	3^+	I	4.9	0.4	0.4
	6.691(V)	0^+	I		c	≤0.1
	6.879(VI)	3^-	0	8.2	0.6	≤0.1
	6.889(VII)	4^+	I	47	2.1	2.1
	8.413(VIII)	4^-	I, VI	−, 3.6	d, 0.9	≈0.1
	9.316(IX)	3^+	I		c	≤0.1
	9.381(X)	2^+	I		c	≤0.1
	9.702(XI)	5^-	I, VI, VIII	24, 4.1, 4.2	0.3, 0.5, 1.0	0.7
	10.377(XII)	$(3)^+$	IV		c	≤0.8
	11.577(XIII)	6^-	XI	5.9	1.1	1.1
^{29}Si	1.273(I)	$\frac{3}{2}^+$	0	13.5	8.6	8.0
	2.028(II)	$\frac{5}{2}^+$	0	3.1	0.4	≤0.2
	2.426(III)	$\frac{3}{2}^+$	0		d	≤2
	3.067(IV)	$\frac{5}{2}^+$	I, II	−, 8	0.5, 0.2	≤0.7
	3.624(V)	$\frac{7}{2}^-$	II	5	0.2	0.2
	4.080(VI)	$\frac{7}{2}^+$	I, II		c	≤0.2
	5.652(VII)	$\frac{9}{2}^+$	IV		c	≤0.7
^{29}P	1.384(I)	$\frac{3}{2}^+$	0		c	≤0.6

[a] σ_γ is the prompt production cross section for a particular γ ray.

[b] σ_x is the cross section for production of a particular state by direct excitation and/or by γ feeding from unidentified higher lying states. γ feeding by transitions from identified higher lying states has been subtracted.

TABLE I. *(Continued)*.

[c] γ rays were not observed. Upper limit for production of excited state was determined.
[d] γ ray masked by a neighboring γ ray. Upper limit for production of excited state was determined.
[e] Excited state which decays by β emission.

IV. DISCUSSION AND CONCLUSIONS

This section will confine itself to observations relating to spectroscopic information concerning the final state channels. General conclusions will be discussed after the relevant heavy fragment evidence has also been introduced in Ref. 8. The Doppler broadening of the γ-ray lines is also best discussed there when the connection with the energy and angular distribution of the detected residual nuclei can be established.

A. Residual nuclei $A \geq 27$

In this section the discrete portion of the light particle spectra are correlated with the γ-ray data. Spectroscopic evidence gained thereby is discussed.

^{30}Si: The very low cross section of $\sigma_p \approx 100$ μb for the observed protons from the ^{27}Al$(\alpha,p)^{30}$Si reaction[7] leading to bound states (or nearly bound states with $E_x \leq 12$ MeV) does not result in adequate statistics to define the levels involved. The γ-ray evidence consists of merely setting an upper limit of $\Sigma \leq 0.5$ mb from the failure to observe any of the expected γ-ray cascades involving the low-lying levels in ^{30}Si.

^{29}Si: The observed deuteron spectrum for $E_d > 110$ MeV from the ^{27}Al$(\alpha,d)^{29}$Si reaction shows the presence of many poorly defined levels below the excitation region of $E_x = 10.8$ MeV. See Fig. 8.

TABLE II. Cross sections deduced from delayed spectra for 140-MeV α particles interacting with ^{27}Al.

Residual nucleus	Daughter nucleus	E_γ (MeV)	σ_γ [a] (mb)	Σ [b] (mb)
^{10}C	^{10}B	0.718	c	≤0.3
^{11}Be	^{11}B	2.125	c	≤0.06
^{13}B	^{13}C	3.853	c	≤0.2
^{14}B	^{14}C	6.094	c	≤0.08
^{14}O	^{14}N	2.314	c	≤0.04
^{15}C	^{15}N	5.299	c	≤0.1
^{16}N	^{16}O	6.129, 7.116	0.62, 0.057	0.9
^{19}O	^{19}F	1.357	1.1	1.1
^{20}O	^{20}F	1.056	0.18	≈0.2
^{20}F	^{20}Ne	1.634	8.8	8.8
^{21}F	^{21}Ne	0.351, 1.395	2.4, 0.3	3.9
^{22}F	^{22}Ne	2.082, 2.165	0.03, 0.03	≈0.05
^{22}Mg	^{22}Na	0.074	c	≤0.5
^{23}Ne	^{23}Na	0.440	2.2	6.7
^{24}Ne	^{24}Na	0.874	c	≤0.8
^{24}Na	^{24}Mg	1.369	19.0	19.1
^{24}Al	^{24}Mg	7.066	c	≤0.15
^{25}Ne	^{25}Na	0.089	c	≤0.3
^{25}Na	^{25}Mg	0.390, 0.975, 1.612	0.8, 0.9, 0.6	6.3
^{26}Na	^{26}Mg	1.809	0.33	0.4
^{26}Si	^{26}Al	0.830	c	≤0.5
^{27}Mg	^{27}Al	0.844, 1.015	7.4, 7.2	7.3
^{28}Mg	^{28}Al	0.401	c	≤0.4
^{28}Al	^{29}Si	1.779	24	24
^{29}Al	^{29}Si	2.426	0.03	≈0.4

[a] Cross section for production of a particular γ ray observed in the delayed spectra.
[b] Cross section for production of a particular residual nucleus after correcting for branching intensity.
[c] Cross section or upper limit determined from failure to observe γ ray in delayed spectrum.

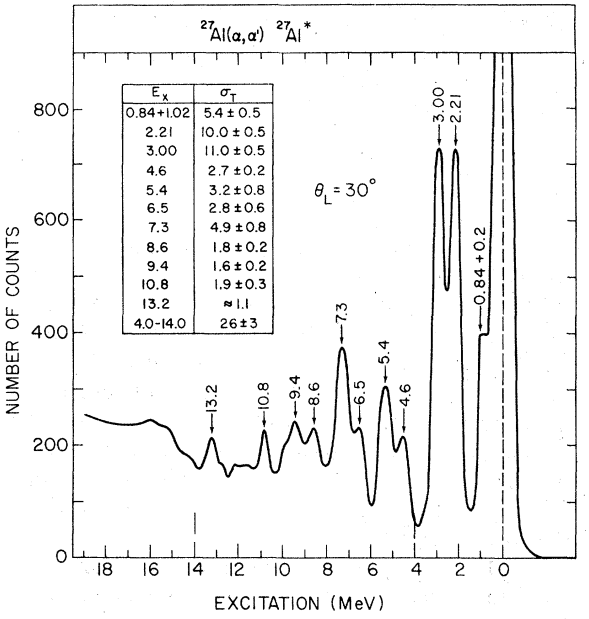

FIG. 5. The discrete energy α'-particle spectrum ^{27}Al(α, α')^{27}Al* observed at θ_L = 30° with E_α = 140 MeV. The angle-integrated total cross sections for the several observed lines are also given. The observed lines are believed to be complex in most cases.

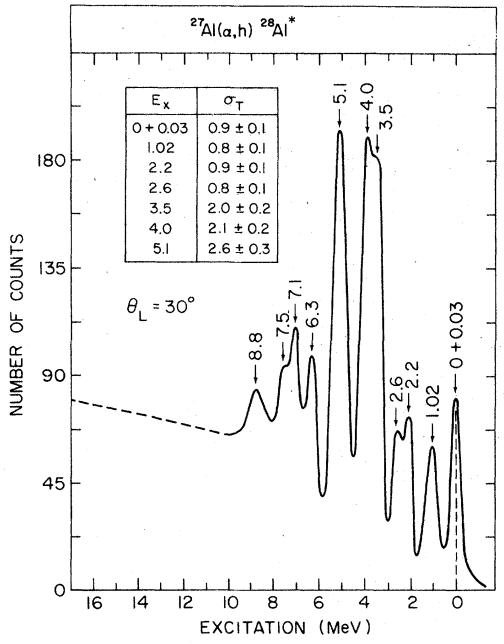

FIG. 6. The discrete energy ^{3}He-particle spectrum ^{27}Al(α,h)^{28}Al* observed at θ_L = 30° with E_α = 140 MeV. Excitation energies in ^{28}Al and corresponding angle-integrated cross sections are also shown.

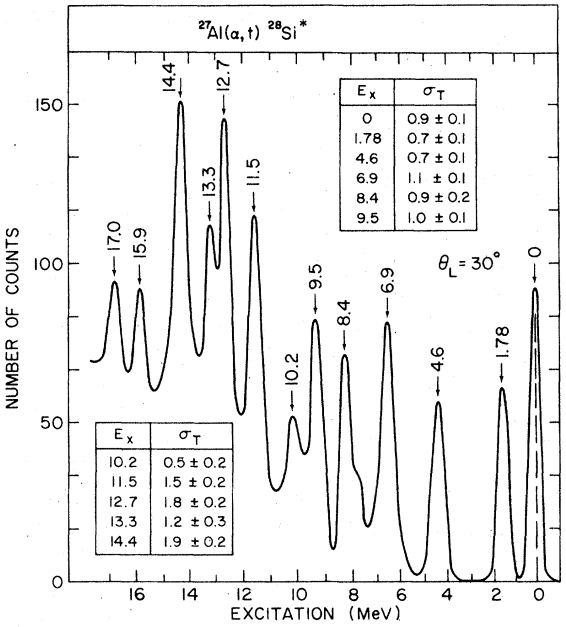

FIG. 7. The discrete energy triton spectrum from ^{27}Al(α,t)^{28}Si* at E_α = 140 MeV and θ_L = 30°. Excitation energies in ^{28}Si and corresponding angle-integrated cross sections are shown.

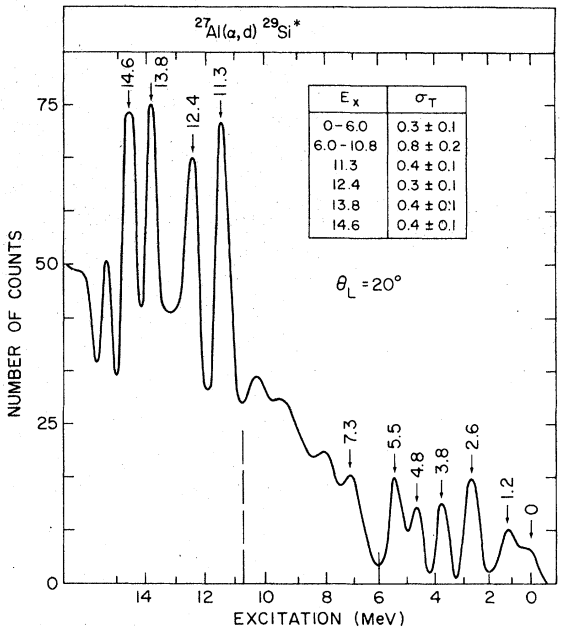

FIG. 8. The discrete energy deuteron spectrum from ^{27}Al(α,d)^{29}Si* at E_α = 140 MeV and θ_L = 20°. Excitation energies in ^{29}Si and corresponding angle-integrated cross sections are shown. The levels below E_x = 6.0 MeV are very poorly defined due to the low statistics, the cross section is only quoted for the sum of all levels below this excitation. The energy region 6.0 < E_x < 10.8 MeV is totally unresolved.

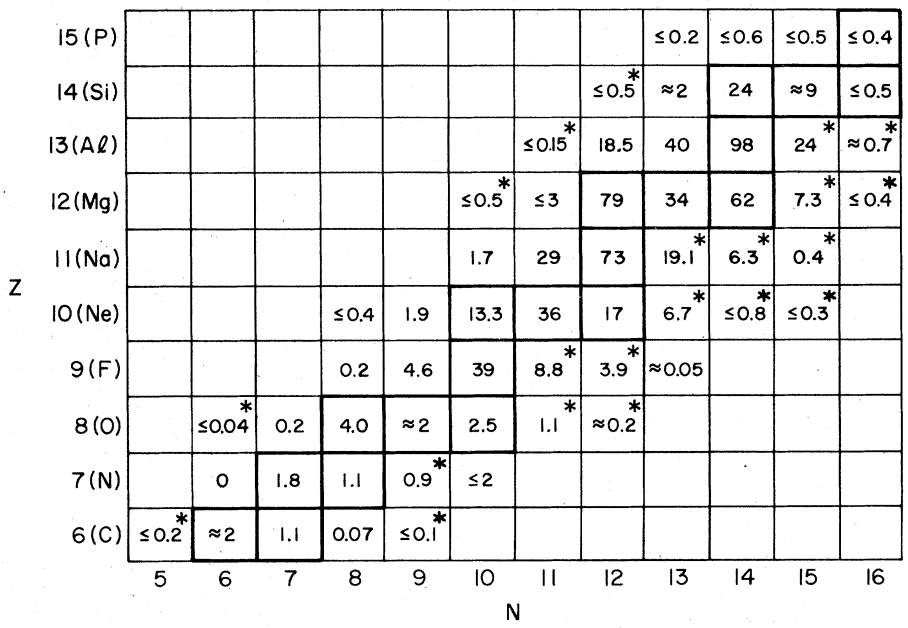

FIG. 9. An N, Z-plot of the gamma-ray-based (GRB)-production cross section of residual nuclei in the inclusive reactions ^{27}Al(α,x) at E_α=140 MeV. All values are in millibarns. These cross sections do not include nuclear processes directly feeding the ground state nor do they include upper limit values or otherwise missed cascading gamma rays. The values for β-decaying nuclei labeled with an asterisk include all production processes since they are based on delayed γ-ray evidence in the daughter nuclei. The total GRB-production cross section for all nuclei exhibited in this figure is Σ_T=695 mb. The absolute errors for all production cross sections is estimated to be 20%.

The total angle-integrated cross section for those deuterons that leave ^{29}Si in bound states is σ_d=1.1 mb. However, the total GRB yield of ^{29}Si is 9.0 mb, thus indicating the need for additional production processes. The observed prominent deuteron lines corresponding to excitations in ^{29}Si greater than 11 MeV (and hence in the continuum) presumably decay by particle emission. Cascading from these states has not been observed.

^{28}Al, ^{28}Si: The first four ^{3}He-particle discrete energy groups observed in the ^{27}Al$(\alpha,h)^{28}$Al reaction may be reasonably correlated with the γ-ray results except for the very much larger yield for exciting the 4$^+$ level at 2.272 MeV, evident in the γ-ray results.

The strongest ^{3}He lines at $E_x\approx$3.5, 4.0, and 5.1 MeV are seen from the γ-ray results to involve the 4$^-$, 5$^-$, 6$^-$ levels in ^{28}Al at E_x=3.465, 4.033, and 5.165 MeV, respectively. One may assume that the three prominent triton lines observed in the parallel ^{27}Al$(\alpha,t)^{28}$Si reaction, indicating level excitations at $E_x\approx$12.7, 13.3, and 14.4 MeV, corresponding to the known T=1 analog states in ^{28}Si with J^π=4$^-$, 5$^-$, 6$^-$ at E_x=12.664, 13.246, and 14.360 MeV, respectively. The cross sections shown in Figs. 6 and 7 for the six lines also lend support to this assumption. These levels have been identified in the literature with possible $(d_{5/2})^{-1}(f_{7/2})^1$ 1p-1h states for the 6$^-$ and 5$^-$ levels, with an additional $(d_{5/2})^{-1}(2p_{3/2})^1$ admixture for the 4$^-$ states, based on observations of the ^{27}Al(d,p), ^{27}Al(d,n), ^{27}Al(p,γ), ^{26}Mg(h,n), ^{28}Si(p,p'), and ^{28}Si(e,e') reactions.[18-24] The *stretched* configuration 6$^-$, $(d_{5/2})^{-1}(f_{7/2})^1$ states have also been identified in other nuclei, for example, in ^{24}Mg at 15.045 MeV.[25]

The observed large cross sections for the transfer of f-shell nucleons to the ^{27}Al core also reflects the presence of the favorable kinematic situation pertaining at E_α=140 MeV. We may readily estimate the maximum or grazing orbital angular momentum in the entrance channel for 140-MeV α particles incident on ^{27}Al to be $L_i\approx 26\hbar$. In event of a strongly forward directed peripheral interaction, the maximum exit channel orbital angular momentum for either ^{28}Si+t or ^{28}Al+h are quite similar and may be estimated to be equal to $L_f\approx 22\hbar$, resulting in a value of $\Delta L = L_i - L_f \approx 4\hbar$. The situation is thus kinematically favorable for the transfer of a nucleon into an f orbital involving $\Delta L = 3\hbar$, since it is possible to achieve both an energy as well as an angular momentum match.

The 4^-, 5^-, and 6^-, $T=1$ levels in ^{28}Si all decay mainly by proton emission and hence no corresponding γ rays are observed. For example, the first of these levels at $E_x=12.664$ appears as a resonance in ^{27}Al(p,γ) experiments[20,24] with $\Gamma_\gamma/\Gamma_p=1.5\times10^{-3}$. The other levels have correspondingly small values of Γ_γ/Γ_p and lifetimes in the range $\tau_m=10^{-20}$ to 10^{-19} s.

The γ-ray results indicate that the 11.5 MeV line observed in the triton spectrum of Fig. 7 corresponds to the known 6^-, $T=0$ level at 11.577 MeV. Although unbound in energy to α-decay to ^{24}Mg, this transition is parity forbidden and the γ decay is readily observed. The other levels of a conjectured $K^\pi=3^-$, $T=0$ rotational band, of which this might be the 6^- member, are also excited. They appear as the lines labeled 6.9, 8.4, and 9.5 MeV. The γ-ray results confirm these assignments and agree with the indication of an excitation cross section more or less monotonically increasing with J as we proceed in excitation from 6.879 MeV, $J^\pi=3^-$; 8.413 MeV, $J^\pi=4^-$; 9.702 MeV, $J^\pi=5^-$ to the level at 11.577 MeV, $J^\pi=6^-$. This effect may also be ascribed to the aforementioned angular momentum matching. The strong, prompt γ-ray line depopulating the 3^- level in Table I with $\sigma_\gamma=8.2$ mb is the result of this cascade.

Although a tempting possibility, the negative parity $T=1$ levels in ^{28}Si and ^{28}Al, and the $T=0$ levels in ^{28}Si do not appear to constitute the 4^-, 5^-, and 6^- members of single rotational bands.[20] Perhaps they represent analog and antianalog intrinsic rotational band heads, based on the coupling of the Nilsson particle orbitals $\frac{3}{2}^-[321]$, $\frac{5}{2}^-[312]$, and $\frac{7}{2}^-[303]$ (members of the generic spherical $f_{7/2}$ state) to the Nilsson hole orbital $\frac{5}{2}^+[202]$. An expected prolate deformation (as exists for the ^{27}Al core) would yield the proper energy sequence and the application of the Gallagher-Moszkowski coupling rule[26] would in each case give the *stretched* angular momentum, namely, $K=\Omega_p+\Omega_h=4^-$, 5^-, and 6^-, respectively. Interband coupling between the higher-energy rotational band members of these intrinsic states would complicate their identification and analysis.

The direct processes (α,h) constitute a total production cross section for bound states of ^{28}Al of $\sigma_h\approx14$ mb. This is to be contrasted to the γ-ray results of $\Sigma=24$ mb from β-decay evidence of the daughter level transitions or the GRB cross section, $\Sigma=20$ mb from the prompt γ rays. The situation involving the various production cross sections for ^{28}Si is similar, the total direct triton cross section is $\sigma_t\approx6.5$ mb, while the GRB-production cross section is $\Sigma=24$ mb.

^{27}Al: The present inelastic α-particle data agrees quite well with that obtained by the Jülich group at the slightly higher energy of $E_\alpha=145$ MeV.[27] The angular distribution suggest $\Delta L=2$ transfer for the lower excitations and an additional admixture of $\Delta L=3$ and perhaps $\Delta L=4$ transfer for the higher excitations. At an elevated incident energy of $E_\alpha=172.5$ MeV, all the lines of Fig. 5 showed multiple structure. The comparison of the (α,α') lines leading to states in ^{27}Al above $E_x=5$ MeV shown in Fig. 5 with possible corresponding levels observed in the ^{24}Mg(α,p) results reported by the Krakow group[28] would suggest high angular momenta for these states.

The γ-ray results are seen to accentuate levels that may be readily associated with the (α,α') line spectra. However, the GRB production cross section for all bound excited states is $\Sigma=98$ mb, while the (α,α') angle-integrated yield below $E_x=8.3$ MeV (the proton separation energy) is $\sigma_\alpha=40$ mb. Since it might be argued that some high-energy γ-ray cascades which might be rather Doppler broadened may be unaccounted for, we may set an absolute upper limit on the yield from the (α,α') channel by integrating all of the spectrum to the rather unrealistically high excitation energy of $E_x=14$ MeV, somewhat above the neutron and α-particle separation energies as well. This still only gives a total value of $\sigma_\alpha\leq52$ mb.

The excess γ-ray production cross sections, when contrasted to the (α,α') particle data, appear to be biased towards the lower excitation energies. The ratio of γ-ray deduced cross sections to the corresponding (α,α') cross sections are $\sigma_\gamma/\sigma_\alpha=5.8$ for the unresolved 0.844 and 1.015 MeV levels, 2.5 for the 2.211 MeV level, 1.9 for the 3.004 MeV level, and approximately unity for the unresolved level complexes above $E_x=4.0$ MeV. If these excess cross sections are due to direct α-particle breakup, this evidence would suggest that this channel predominantly leaves ^{27}Al with little excitation. This is also basically in agreement with the production cross section results for ^{28}Si, in which the first excited state showed the major excess γ-ray yield and perhaps even for ^{28}Al where the 4^+ state at $E_x=2.272$ MeV might play the major role in providing the observed excess.

A careful search for γ-ray cascades from possible negative parity states comprising the reported octupole-strength[29] concentration in the range $E_x=4.0$ to 14.0 MeV failed definitively to identify any. Table I shows a few upper limits in those cases where regardless of the background and the proximity of other lines relatively tight values could be set. In the vicinity of $E_x\approx7.3$ MeV where judging from the (α,α') data the strongest possibility for such levels is expected only

the $\frac{9}{2}$ level of unknown parity at $E_x = 7.399$ MeV is a possible candidate. (If correctly identified, its lifetime would also be predicted to be $\tau_m \leq 100$ fs from the γ-ray data.) Particle-γ-ray coincidence studies are required to examine this situation.

In all cases for the production of residual nuclei $A \geq 27$ the total GRB-production cross sections exceed the values deduced from the high-energy portion of the p, d, t, h, and α spectra lying at particle energies above the appropriate excitation thresholds. A possible source for additional production contributions might be from γ-ray cascading from continuum to bound states. High angular momentum states may be initially excited in the heavy fragments leading at first to some γ-ray cascading. However, such cascading will eventually be damped by particle emission prior to reaching the bound state region.[1]

It might also be possible for pre-equilibrium plus evaporation processes to lead to bound state residual nuclei accompanied by multiparticle emission thus explaining the difference in yields. To estimate these contributions model calculations were performed. These model calculations, discussed in detail in Ref. 8, fail to give adequate yields for residual nuclei in this mass region. Such calculations predict yields of 0.5 mb for ^{29}Si, 2.0 mb for ^{28}Al, 9.3 mb for ^{28}Si, and 35.3 for ^{27}Al. These yields are far too small.

Finally, the only process remaining which could give contributions missed in the particle spectra and also not be included in the model codes is projectile-fragmentation contributions. Such processes are known to occur with significant cross sections.[30]

B. Direct excitations and cluster effects

Perhaps the most striking feature of the γ-ray data is the observation that all the anomolously large cross sections for each residual nucleus are associated with individual levels that may be generically related. Those states having short-enough life times also show large Doppler effects for the resulting γ rays. The sum total of all such identified cross sections is estimated to be ≈ 300 mb out of a total reaction cross section of $\sigma_R = 1150$ mb. Since the reaction processes that involve pre-equilibrium steps followed by evaporation stages would be expected to populate residual nuclear states governed by a statistical distribution, such processes could not account for these observed results. Further, as a general rule these processes would not necessarily involve recoil velocities leading to large Doppler effects. The prominent observed excitations are therefore assigned to be the results of prompt processes.

The following subsections, arranged by nuclear species that exhibit possibly related excitation processes, summarize conjectured spectroscopic characteristics. These include largely literature based contentions as well as some that are presently suggested.

^{28}Al, ^{22}Ne, and ^{22}Na: γ-ray evidence indicates that the 4^+, 2.272 MeV level in ^{28}Al is strongly excited. This level while present in the discrete ^{3}He spectrum shown in Fig. 6 is a low yield member of a doublet. This level also appears in the ^{27}Al(d,p) stripping reactions with $l_n = 2$. A simple structure for this level would be the stretched coupling of a $(d_{3/2})$:$\frac{3}{2}^+[202]$ neutron and a $\frac{5}{2}^+[202]$ proton hole giving a 4^+ state. This structure would parallel the prominent 6^- stretched $f_{7/2}$ neutron state. The largest production cross sections for ^{22}Ne and ^{22}Na are to the 2^+, $T = 1$ pair of analog states. If these yields are associated with the $(\alpha, {}^9B^*)$ and $(\alpha, {}^9Be^*)$ pick up processes, both levels should have important 2p-2h components consisting of a coupled pair or nucleons in the $\frac{5}{2}^+[202]$ Nilsson orbital.

^{27}Al, ^{23}Na, and ^{19}F: Reference to Table I shows that among the odd-A nuclei ^{27}Al, ^{23}Na, and ^{19}F have relatively large local GRB-production cross sections. These three may be strongly fed by (α,α'), $(\alpha,2\alpha)$, and $(\alpha,3\alpha)$ processes. There appears to be a high spectroscopic selectivity in the individual states populated.

Among the simplified models for the level structure of ^{27}Al the Jülich group[27] suggest a relatively successful rotational-vibrational model in competition to the usual weak coupling model that attempts to describe the low lying states in terms of a $d_{5/2}$ hole in ^{28}Si. They associate the $\frac{7}{2}^+$, 2.211 MeV level and the $\frac{9}{2}^+$, 5.432 MeV level with the ground state $K^\pi = \frac{5}{2}^+$ band head (presumably based on the $\frac{5}{2}^+[202]$ Nilsson orbital). Two γ-vibrational band heads are place at 3.004 MeV with $K^\pi = (\frac{5}{2}+2)^+ = \frac{9}{2}^+$, and at 0.844 MeV with $K^\pi = (\frac{5}{2}-2)^+ = \frac{1}{2}^+$. The first γ-band sequence identifies the $\frac{11}{2}^+$, 4.510 MeV level as its next rotational member, while the latter sequence continues with the levels $\frac{3}{2}^+$, at 1.015 MeV and $\frac{5}{2}^+$, at 2.734 MeV. Also this latter $K^\pi = \frac{1}{2}^+$ band, it is suggested, may be mixed with the intrinsic Nilsson $\frac{1}{2}^+[211]$ orbital state. A band head at 2.981 MeV with $K^\pi = \frac{3}{2}^+$, and its next rotational member state $\frac{5}{2}^+$, at 4.409 MeV may be associated with either the Nilsson $\frac{3}{2}^+[202]$ or $\frac{3}{2}^+[211]$ intrinsic orbital states.

We note that the most strongly populated states in ^{27}Al are in fact the ground state band and its γ-vibration counterpart band members that may be reached by coupling a single quadrupole-phonon excitation to the ground state. The strongly populated $\frac{1}{2}^+$, 0.844 MeV and $\frac{9}{2}^+$, 3.004 MeV levels in

^{27}Al are expected to have components of the 2^+ vibration state in ^{28}Si coupled to a $d_{5/2}$ hole and the corresponding 2^+ state in ^{26}Mg coupled to $d_{5/2}$ particle. Indeed the lowest 2^+ states in ^{26}Mg and ^{28}Si are also strongly excited.

In the production cross section of ^{23}Na the largest intensities are to the lowest $\frac{7}{2}^+$ and $\frac{9}{2}^+$ states as in the case of ^{27}Al, and with strikingly comparable magnitudes. Although no cluster model analysis for ^{23}Na exists in the literature, these states in ^{23}Na are conjectured to have significant triton cluster components involving three nucleous in the $\frac{5}{2}^+[202]$ Nilsson orbital. The very large Doppler broadening of the γ rays in Table I originating with short-lived levels ($\tau_m < 100$ fs) is most readily accounted for by assuming an α transfer reaction ^{27}Al(α,^{8}Be)^{23}Na with the subsequent breakup of the ^{8}Be, or alternatively a tight (α,2α) spallation shower, see Ref. 8.

If the $K^\pi = \frac{1}{2}^-$, 2.640 MeV band head in ^{23}Na and its rotational members $\frac{3}{2}^-$, 3.678 MeV and $\frac{5}{2}^-$, 3.848 MeV are based on a p-shell hole in the Nilsson orbital $\frac{1}{2}^-[101]$, their low production cross section compared to the above levels is understandable, since these states would have very little in common with the $(2s_{1/2}d_{5/2})^3$ cluster states.

Similarly the major production cross sections for the residual nucleus ^{19}F also involve the well known rotational band states based on the triton cluster ground state.[31] The strikingly large population cross section of 30 mb for the lowest $\frac{5}{2}^+$ level is notable, contrasted to the order of magnitude smaller population of the $K^\pi = \frac{1}{2}^-$ band based on the known ^{15}N + α cluster states. This may be taken as an indication of a considerable admixture of the state involving three nucleons in the $\frac{5}{2}^+[202]$ Nilsson orbital for the $\frac{5}{2}^+$ state.

^{28}Si, ^{24}Mg, and ^{20}Ne: Rather large GRB production cross sections are observed for these residual nuclei. After allowing for all observed cascading, the dominant production strength in each instance is to the first excited 2^+ state. If the suggestion of a direct channel breakup of the α particle for the excess production of ^{28}Si largely in the 2^+ state is accepted, the rather large transitions to the 2^+ levels in ^{24}Mg and ^{20}Ne might also be expected to result from a direct process, perhaps leaving the lighter mass component fragmented. Highly excited cluster knockout or transfer components might be involved such as (α,t*), (α,^{7}Li*), (α,^{11}B*). The small but non-negligible yield of p-shell recoil nuclei is discussed in Ref. 8. This low yield is such as to suggest that if p-shell nuclei are in fact initially produced they mostly fragment or their component parts simply leave as a spallation shower.

^{16}O, ^{15}O, and ^{15}N: The only prompt γ ray attributed to ^{16}O is from the 3^- level at $E_x = 6.129$ MeV. Wang and Shakin[32] have found it necessary to assign an important 3p-3h admixture to low lying negative parity states in ^{16}O particularly in the giant dipole region of excitation. There is also a suggestion of $\approx$18% $(2s1d)^3$ 3p-3h admixture in the 3^- level as well. Thus the excitation of this level may be seen as dependent on the admixture of the initial $(2s1d)^3$ configuration.

The only prompt γ rays definitely observed in ^{15}O and ^{15}N are from the lowest $\frac{3}{2}^+$ pair of analog states. The readily observed γ ray from the unnatural parity $\frac{5}{2}^+$ first excited state in ^{15}N, if not the result of undetected cascading, may be taken to indicate a possible $(2s_{1/2}d_{5/2})^3$ triton cluster component in this level. Theoretical three-particle cluster configurations of shell model $(2s_{1/2}d_{5/2})^3$ variety coupled to a ^{12}C core have been successfully applied for the higher excited states in ^{15}N, the $\frac{5}{2}^+$ first excited state has been generally considered adequately accounted for as a ^{12}C core coupled to a $(1p_{1/2})^2(2s_{1/2}d_{5/2})^1$ three-particle cluster.[33,34] The three nucleon transfer reaction ^{12}C(α,p)^{15}N at Jülich has, however, definitely established a $(2s1d)^3$ component in the two lowest excited states.[35] Of the four analog states, $\frac{1}{2}^+$, $\frac{5}{2}^+$, in ^{15}O and $\frac{1}{2}^+$, $\frac{5}{2}^+$ in ^{15}N, the γ-ray yield σ_γ is several times stronger for the decay of the $\frac{3}{2}^+$ state in ^{15}N than the other three. This again may be taken as reflecting a strong parentage with the initial $(2s1d)^3$ configuration in the target nucleus ^{27}Al ground state.

^{27}Al, ^{25}Al, ^{25}Mg, and ^{21}Ne: The striking similarity of the level structure of ^{27}Al (and ^{27}Si) on the one hand and ^{25}Al and ^{25}Mg on the other is presumed to be related to the presence of corresponding Nilsson hole and Nilsson particle states. For example, the ground state band heads $K^\pi = \frac{5}{2}^+$ in ^{27}Al and ^{27}Si are based on the intrinsic hole state $\frac{5}{2}^+[202]$, while that of ^{25}Al and ^{25}Mg are based on the intrinsic particle state $\frac{5}{2}^+[202]$. It might then be expected that direct transfer reactions ^{27}Al(α,^{6}Li*)^{25}Mg or ^{27}Al(α,^{6}He*)^{25}Al or possibly equivalent direct spallation showers would populate ^{27}Al related levels in ^{25}Al and ^{25}Mg. The first four levels in ^{25}Mg are populated with cross sections in the range 0.5 to 0.2 times the corresponding states in ^{27}Al. Compare entries in Table I. Although the lowest $\frac{7}{2}^+$ state in ^{25}Al is the strongest excitation as in ^{27}Al and ^{25}Mg, the remaining correlation in excitation strengths is not as close as that between ^{25}Mg and ^{27}Al.

The strongest excitations in ^{21}Ne are the lowest $\frac{7}{2}^+$ and $\frac{9}{2}^+$ levels. These states must have a complexity beyond the coupling of a single neutron to the ^{20}Ne ground state. At a minimum the 2^+ ^{20}Ne

core state of a 3p-3h state is required.

The above spectroscopic information will be discussed in terms of a possible comprehensive model in Part II.

The authors wish to thank Dr. N. R. Yoder for his help with software programming. A grant from the University of Maryland Computer Science Center for carrying out some calculations is acknowledged. This work was supported in part by the National Science Foundation.

---

*Present address: Research Reactor Facility, University of Missouri, Columbia, Missouri 65201.
†Present address: IBM Corporation, Poughkeepsie, New York 12602.

[1]W. F. Hornyak, M. D. Glascock, C. C. Chang, and R. J. Quickle, Technical Report No. 78-082, University of Maryland, 1978 (unpublished).
[2]W. F. Hornyak, M. D. Glascock, C. C. Chang, and J. R. Wu, Technical Report No. 78-083, University of Maryland, 1978 (unpublished).
[3]J. J. Griffin, Phys. Rev. Lett. 17, 478 (1966); M. Blann, *ibid.* 21, 1357 (1966).
[4]H. W. Bertini, Phys. Rev. 131, 1801 (1963).
[5]J. R. Wu and C. C. Chang, Phys. Rev. C 16, 1812 (1977).
[6]M. Blann, Phys. Rev. Lett. 27, 337 (1971); M. Blann and A. Mignerey, Nucl. Phys. A186, 245 (1972).
[7]J. R. Wu, C. C. Chang, and H. D. Holmgren, Phys. Rev. C 19, 659 (1979).
[8]W. F. Hornyak, M. D. Glascock, C. C. Chang, and J. R. Wu, following paper.
[9]C. O. Butterfield and N. R. Yoder (unpublished).
[10]H. Seyfarth, A. M. Hassan, B. Hrastnik, P. Gottel, and W. Delang, Nucl. Instrum. Methods 105, 301 (1972).
[11]H. Seyfarth, Nucl. Instrum. Methods 114, 125 (1974).
[12]E. Vãno, L. Gonzalez, R. Gaeta, and J. A. Gonzalez, Nucl. Instrum. Methods 123, 573 (1975).
[13]N. R. Yoder, C. C. Chang, R. J. Quickle, and M. D. Glascock (unpublished).
[14]M. A. Mariscotti, Nucl. Instrum. Methods 50, 309 (1967).
[15]F. Ajzenberg-Selove and T. Lauritsen, Nucl. Phys. A227, 1 (1974); F. Ajzenberg-Selove, *ibid.* A248, 1 (1975); A281, A268, 1 (1977); A300, 1 (1978).
[16]P. M. Endt and C. van der Leun, Nucl. Phys. A214, 1 (1973).
[17]R. J. de Meijer, H. S. Plendl, and R. Holub, Nucl. Data Tables 13, 1 (1974); R. J. de Meijer, A. G. Drentje, and H. S. Plendl, *ibid.* 15, 391 (1975).
[18]R. M. Freeman, F. Haas, A. R. Achari, and R. Modjtahed-Zadeh, Phys. Rev. C 11, 1948 (1975).
[19]C. Miehé, A. Huck, G. Klotz, and G. Walter, Phys. Rev. C 15, 30 (1977).
[20]J. Dalmas, F. Leccia, and M. M. Aléonard, Phys. Rev. C 9, 2200 (1974).
[21]F. A. El-Akad, S. Backe, T. Holtebekk, F. Ingebretsen, and J. Rekstad, Nucl. Phys. A283, 12 (1977).
[22]T. W. Donnely, Jr., J. D. Walecka, G. E. Walker, and I. Sick, Phys. Lett. 32B, 545 (1970).
[23]G. S. Adams, A. D. Bacher, G. T. Emery, W. P. Jones, R. T. Kouzes, D. W. Miller, A. Picklesimer, and G. E. Walker, Phys. Rev. Lett. 38, 1387 (1977).
[24]G. F. Neal and S. T. Lam, Phys. Lett. 458, 127 (1973).
[25]H. Zarek, B. O. Pich, T. E. Drake, D. J. Rowe, W. Bertozzi, C. Creswell, A. Hirsch, M. V. Hynes, S. Kowalski, B. Norum, F. N. Rad, C. P. Sargent, C. F. Williamson, and R. A. Lindgren, Phys. Rev. Lett. 38, 750 (1977).
[26]C. J. Gallagher and S. A. Moszkowski, Phys. Rev. 111, 1282 (1958).
[27]K. T. Knöpfle, A. Kiss, M. Rogge, U. Schwinn, P. Turek, O. Aspelund, and C. Mayer-Böricke, Phys. Rev. C 13, 1400 (1976).
[28]R. Zybert, A. Budzanowski, J. Plaskonka, I. Skwirczynska, A. Strzalkowski, and L. Zybert, Nucl. Phys. A277, 15 (1977).
[29]C. Mayer-Böricke, W. Oelert, A. Kiss, M. Rogge, P. Turek, and S. Wiktor, Nucl. Phys. A293, 189 (1977).
[30]J. R. Wu, C. C. Chang, and H. D. Holmgren, Phys. Rev. Lett. 40, 1013 (1978).
[31]B. Buck and A. A. Pilt, Nucl. Phys. A280, 133 (1977).
[32]W. L. Wang and C. M. Shakin, Phys. Rev. C 5, 1898 (1972).
[33]B. Buck, C. B. Dover, and J. P. Vary, Phys. Rev. C 11, 1803 (1975).
[34]J. Bommer, M. Ekpo, H. Fuchs, K. Grabisch, and H. Kluge, Nucl. Phys. A251, 246 (1975).
[35]W. R. Falk, A. Djaloeis, and D. Ingham, Nucl. Phys. A252, 452 (1975).